ARTICLES

Direct Observation of OH Formation and Luminescent Emission from Photoexcited Acetaldoxime

Pradyot K. Chowdhury

Radiation Chemistry and Chemical Dynamics Division, Bhabha Atomic Research Centre, Trombay, Mumbai−400 085, India

Received: June 14, 2002; In Final Form: September 17, 2002

On photoexcitation at 193 nm, the $^1(\pi, \pi^*)$ excited acetaldoxime ($CH_3-CH{=}N-OH$) appears to be undergoing intersystem crossing producing a highly energized triplet state, which is followed by parallel processes of the emission of a UV photon at 310 nm and the dissociation to $CH_3-CH{=}N$ and OH radicals as primary products. While the laser-induced fluorescence showed that only 1.5% of the nascent OH ($X^2\Pi$) is produced in the vibrationally excited state with $v = 1$, there is no OH produced with $v = 2$. The rotational state distribution of OH is found to fit a Boltzmann distribution, characterized by a rotational temperature T_{rot} of 1200 ± 120 K for the $v = 0$ and T_{rot} of 990 ± 100 K for the $v = 1$ vibrational states, respectively. By measuring the Doppler spectroscopy of the $v = 0$ and $v = 1$ states of OH, the translational energy of the photofragments is found to be 40.0 ± 5.0 and 32.2 ± 4.0 kcal mol^{-1}, respectively. While 20 kcal mol^{-1} of translational energy is expected statistically, imparting such a large amount of translational energy into the products suggests that the dissociation occurs on the excited state potential energy surface. The real time formation of OH shows a dissociation rate of the acetaldoxime to be (1.5 ± 0.3) × 10^6 s^{-1}. The above dissociation rate vis-à-vis statistical Rice−Ramsperger−Kassel−Marcus theory suggests that the acetaldoxime dissociates from the triplet state, with a threshold dissociation energy of about 49 kcal mol^{-1}. The decay of the triplet acetaldoxime emission at 310 nm with a rate of (1.2 ± 0.3) × 10^6 s^{-1}, similar to that of its dissociation to form OH, further suggests that both the competitive decay processes occur from the triplet state potential energy surface.

1. Introduction

The dynamics of photodissociation following electronic excitation of small molecules have been studied extensively,[1−5] where dissociation occurs on a time scale comparable to that of molecular vibrations (<1 ps). The long time required for molecular dissociation in the ground electronic state produced via internal conversion ensures that the dissociation time scale of the molecule corresponds to the predictions of the statistical unimolecular reaction rate theory. Our recent study on the photodissociation of furfuryl alcohol[6] and 1,4-pentadien-3-ol[7] is considered to be such an example of the molecular dissociation after internal conversion. However, we have reported the instanteneous C−C bond dissociation from Rydberg-excited hydroxyacetone[8] following the absorption of a 193 nm photon, whereas a slower dissociation of the C−O bond has been reported from the triplet surface,[9] on exciting the $^1(n, \pi^*)$ state of hydroxyacetone at 248 nm. Similarly, a nanosecond dissociation time scale of acetone on the excited singlet surface has recently been observed by Diau et al.[10,11] Dagdigian et al.[13] studied the laser-induced fluorescence (LIF) of the OH fragments produced from photolysis of oximes at 193 nm. To see whether the electronic excited state or the ground state is responsible for the photodissociation reaction, we have studied acetaldoxime by exciting the $^1(\pi, \pi^*)$ state at 193 nm.

The work reported here is that on photoexcitation at 193 nm; the $^1(\pi, \pi^*)$ excited acetaldoxime ($CH_3-CH{=}N-OH$) appears to be undergoing rapid intersystem crossing (ISC) producing a highly energized triplet, which is followed by parallel processes of the emission of a UV photon at 310 nm and the dissociation to $CH_3-CH{=}N$ and OH radicals as primary products. The dissociation rate of acetaldoxime vis-à-vis statistical Rice−Ramsperger−Kassel−Marcus (RRKM) theory suggests that the triplet state acetaldoxime dissociates with a threshold dissociation energy of about 49 kcal mol^{-1}, which is lower than that of the ground state threshold dissociation energy of 67 kcal mol^{-1}. Observation of the decay rate of the acetaldoxime emission at 310 nm, similar to that of its dissociation to form OH, suggests that both of the competitive decay processes occur from the triplet state potential energy surface.

Moreover, the OH radical has a rich rovibrational spectroscopy and is suitable for the determination of product energy distributions. Some information on the dissociation dynamics of acetaldoxime can be obtained from the nascent initial state distribution of the products, e.g., OH (v, N, f), where v is the

* To whom correspondence should be addressed. Fax: +91-22-5505151. E-mail address: cpradyot@yahoo.com.

10.1021/jp026309h CCC: $22.00
Published on Web 10/16/2002

vibrational quantum number, N is the rotational quantum number, and f refers to one of the four OH fine structure levels.

2. Experimental Section

The schematic of the laser photolysis−LIF setup (LP−LIF) used in the present study and the details of the experimental procedures are given in our earlier publications,[6−9] and a brief account is as follows. The photolysis laser employed is an excimer laser (Lambda Physik model Compex-102, Fluorine version), and the probe laser is a Quantel dye laser with frequency doubling and mixing module (TDL 90) pumped by Quantel seeded Nd:YAG laser (model YG 980 E-20). The reaction chamber is made up of stainless steel with crossed right angle arms for photolysis and probe lasers. All of the arms are equipped with baffles, and the windows are fixed at the Brewster angle to decrease scattering. The photolysis and the probe lasers intersect at the center of the reaction cell. The detection system views at right angle the intersection volume of photolysis and probe laser through the bottom arm window. The fluorescence is collected by a 38 mm diameter lens of focal length 50 mm and detected by a PMT (Hamamatsu model R 928P). A bandpass filter ($\lambda_{center} = 310$ nm, full width at half-maximum (fwhm) $= \pm 10$ nm, $\%T_{310\ nm} = 10\%$) is placed between the collecting lens and the PMT to cut off the scattering from the photolysis laser. The fluorescence signal is gate-integrated by a boxcar (SRS 250), averaged for 30 laser shots and fed into an interface (SRS 245) for A/D conversion. A Pentium II PC is used to control the scan of the dye laser via RS232 interface and to collect data through the GPIB interface using control and data acquisition programs. The fluorescence intensities are normalized for laser intensity fluctuations of the pump and the probe lasers monitored by photodiodes.

In the present work, acetaldoxime vapor was flowed through the reaction chamber at a flow velocity of approximately 10 cm/sec and photolyzed at 193 nm. The pressure of acetaldoxime was maintained at about 10 mTorr. The OH fragment was probed state selectively by exciting the $A^2\Sigma \leftarrow X^2\Pi$ (0,0) transition of OH at 307−314 nm and (1,1) transition of OH at 313−316 nm, respectively, and followed by monitoring the total $A \rightarrow X$ fluorescence. The laser frequency was calibrated using the optogalvanic signal of a hollow cathode lamp with an accuracy of ± 0.3 cm^{-1}. The spectral resolution of the probe laser was 0.06 cm^{-1}. Both of the laser beams used are unfocused and attenuated further to prevent saturation. The measured LIF signal was found to be linearly proportional to the laser power.

On 193 nm excitation of acetaldoxime, a weak emission in the UV region was observed. We tried to obtain the emission spectrum with another detection system, which consisted of a collecting lens, a monochromator, and a PMT. Because of weak emission intensity, the spectrum was not satisfactory. However, the emission temporal profile was taken at 310 nm with a bandpass filter (fwhm $= \pm 10$ nm) to estimate the lifetime of the emitting species. Acetaldoxime (99% purity, Fluka) was freeze-pump-thawed five times prior to use.

3. Results and Discussion

Acetaldoxime undergoes a simple bond fission reaction producing two radicals, $CH_3-CH{=}N$ and OH, as follows

$$CH_3-CH{=}N-OH \rightarrow CH_3-CH{=}N + OH \quad \Delta H^\circ = 66.6 \text{ kcal mol}^{-1} \quad \text{(I)}$$

There is considerable uncertainty in the $CH_3(H)CN-OH$ bond dissociation energy. The value 48.4 kcal mol^{-1} reported by Benson and O'Neal[12] from the available experimental unimolecular decay kinetic data appears to be too low, where the authors questioned the validity of the experimental data. The N−O bond dissociation energy of 66.6 kcal mol^{-1} reported recently by Dagdigian et al.[13] by observing a general trend in the bond dissociation energy of small oximes seems quite reasonable, and we have used this value.

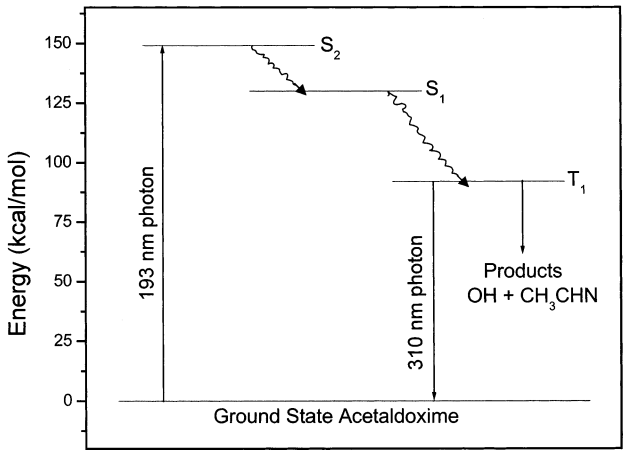

Figure 1. Schematic energy level diagram of the 193 nm photodissociation of acetaldoxime.

On irradiation of acetaldoxime at 193 nm, a rate constant, $k = 1.5 \times 10^6$ s^{-1}, has been estimated from the real time formation of OH. While the energy barrier on the singlet excited surface may prohibit its dissociation, the vibrationally excited ground electronic state acetaldoxime, if formed by internal conversion, would be dissociating at a RRKM predicted rate of 10^{10} s^{-1}. Therefore, it appears that the singlet $^1(\pi, \pi^*)$ excited acetaldoxime undergoes ISC to the triplet state, followed by dissociation generating $CH_3-CH{=}N$ and OH radicals. A schematic energy level diagram of the 193 nm photodissociation of acetaldoxime is depicted in Figure 1.

3.1. Rotational State Distribution of Nascent OH by LIF. The formation of OH radicals was observed in the irradiation of acetaldoxime by a pulsed ArF excimer laser. Typical LIF signals from OH exhibited simple exponential decays, with decay times consistent with OH $A^2\Sigma^+$ state measurements. A typical LIF spectrum of the OH observed at a probe time of 100 ns after the excimer laser pulse and a acetaldoxime pressure of 10 mTorr are shown in Figure 2. At this pressure, the hard sphere collision rate is 10^5 s^{-1} molecule^{-1}, which ensures that no collisional relaxation occurred within the probe time of 100 ns. The line assignment and nomenclature are based on the extensive spectroscopic work of Dieke and Crosswhite.[14] All of the peaks in Figure 2 correspond to transitions originating in the $X^2\Pi_i$ ($v = 0$) level. Normally, relative peak areas of the rotational lines of LIF signals were used to obtain relative OH densities. Conversion of the measured LIF signal S to a state-resolved OH($X^2\Pi$) population requires correction for variations in the intensity of both the ArF and the probe lasers I_{photol} and I_{probe}, as well as accurate values of the Einstein coefficients, B_{ik} for the $k \leftarrow i$ transition at ν_{ik}.

$$P(v'',N'',f'',\lambda'') = (S/I_{photol}I_{probe}B_{ik}v_{ik}) \qquad (1)$$

The pump and probe laser intensity variation was monitored simultaneously with the LIF signal during spectral scan. Tabulated values of B_{ik} are used throughout.[15] Here, the energy of the probe laser (maximum energy about 10 mJ/pulse) was reduced by a factor of 1000 to ensure a linear response of the

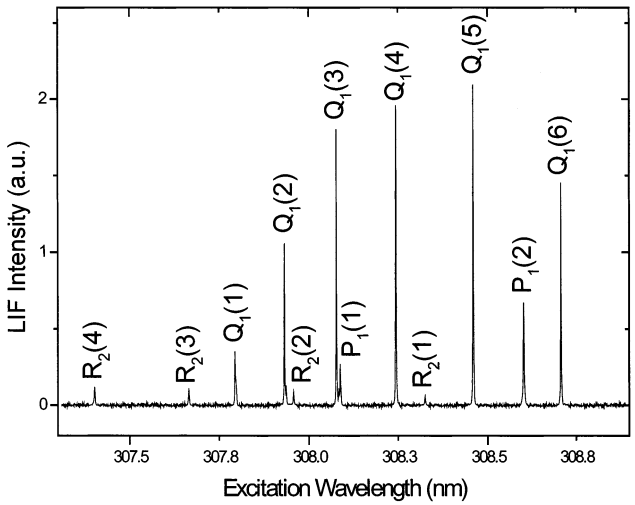

Figure 2. Portion of the LIF rotational excitation spectrum of OH radical formed in the irradiation of acetaldoxime by an ArF excimer laser (20 ns, 150 mJ/pulse). The acetaldoxime pressure used is 10 mTorr, and the delay between the ArF and the dye laser is 100 ns. The spectral assignments are based on ref 14.

fluorescence to laser power. Conversion of the spectrum to micropopulations is obtained by dividing the state populations by their rotational degeneracy, $(2J'' + 1)$. A Boltzmann plot of rotational states, i.e., ln $[P(J)/(2J + 1)]$ vs E_R, the rotational energy of the state, is shown in Figure 3a. The straight line is the computer least-squares fit of the data, representing different Λ ($^2\Pi^+$, $^2\Pi^-$) and spin−orbit ($^2\Pi_{3/2}$, $^2\Pi_{1/2}$) states. They seem to have approximately the same Boltzmann distribution, characterized by a common rotational temperature (T_R) of 1200 ± 120 K. This measured distribution of initial rotational states corresponds to an average rotational energy in OH, $E_R = 2.4$ kcal mol^{-1}. A second set of experiments was carried out to cross-check and determine $P(J)$ for OH($^2\Pi$) states, which gave an identical result for T_R.

To measure the rotational temperature of the OH produced in the $v'' = 1$ level, the LIF scan was continued through the (1,1) vibrational transition up to the $P_1(6)$ rotational line. A Boltzmann plot of rotational states, i.e., ln $[P(J)/(2J + 1)]$ vs E_R, the rotational energy of the state, is shown in Figure 3b. The straight line fit of the data, representing different Λ ($^2\Pi^+$, $^2\Pi^-$) and spin−orbit ($^2\Pi_{3/2}$, $^2\Pi_{1/2}$) states, seems to have approximately the same Boltzmann distribution, characterized by a common rotational temperature (T_R) of 990 ± 100 K. This measured distribution of initial rotational states corresponds to an average rotational energy in OH, $E_R = 2.0$ kcal mol^{-1}. By integrating the population of the rotational states in the $v' = 1$ and $v'' = 0$ bands, about 1.5% of the OH is found to be produced in the $v'' = 1$ state. This corresponds to a vibrational temperature of the OH radicals to be $T_V = 1240 \pm 120$ K.

3.2. Translational Energy of OH from Doppler Line Width. The component of OH fragment velocity along the probe laser propagation axis z, v_z, shifts the central absorption frequency ν_0 to ν by the following equation:

$$\nu = \nu_0(1 \pm v_z/c) \qquad (2)$$

where c is the velocity of light. The line width and shape of the Doppler-broadened LIF line includes contributions from the fragment molecular velocity, the thermal motion of the parent, and the finite probe laser line width. The peak profile for $P_1(5)$ is shown in Figure 4a. All of the rotational lines are seen to exhibit the same line width within the experimental error. For

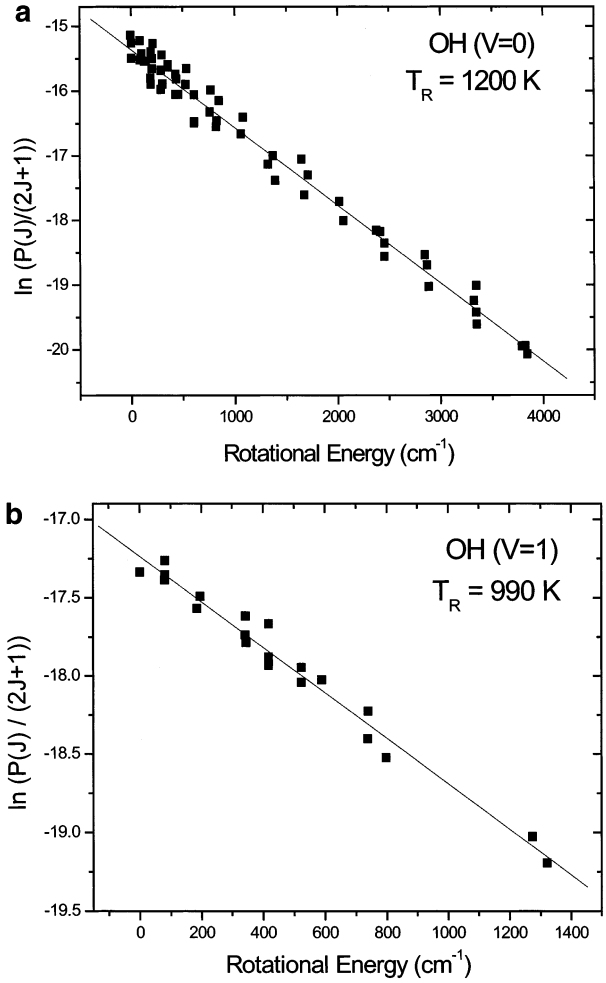

Figure 3. (a) Boltzmann plot of the $v = 0$ populations in various microstates of nascent OH. The distribution of four different spin and Λ doublet states of OH is characterized by a temperature, $T^R = 1200 \pm 120$ K. (b) Boltzmann plot of the $v = 1$ populations in various microstates of nascent OH. The distribution of four different spin and Λ doublet states of OH is characterized by a temperature, $T^R = 990 \pm 100$ K.

a completely isotropic OH fragment velocity distribution, the deconvolution of the peak profiles with the instrumental function gives the Doppler width as 0.51 ± 0.03 cm^{-1}. For the Maxwell−Boltzmann translational energy distribution, this corresponds to an average relative translational energy of 39.8 ± 5.0 kcal mol^{-1} in the center of mass coordinate of the photofragments, after due correction for the thermal energy of the parent. We have assumed a Gaussian profile for the velocity distribution, which fits quite well with the observed velocity distribution.

To see the Doppler profile in the vibrationally excited OH, the peak profile for $P_1(5)$ of the (1,1) transition is scanned, which is shown in Figure 4b. This band shape also fits well with the Gaussian function, giving a Doppler width of 0.45 ± 0.03 cm^{-1}. For the Maxwell−Boltzmann translational energy distribution, this corresponds to an average relative translational energy of 32.2 ± 4.0 kcal mol^{-1} in the center of mass coordinate of the photofragments.

3.3. Kinetics of Acetaldoxime Dissociation. The production of OH($v'' = 0$) as a function of the delay time between the two lasers was obtained by monitoring the intensity of the $Q_1(5)$ LIF signal as shown in Figure 5. The buildup of the signal was found to be rapid during a few hundred nanoseconds after the photolysis laser pulse, whereas a slower decay was observed up to 1.5 μs afterward. The first data point was taken at a probe

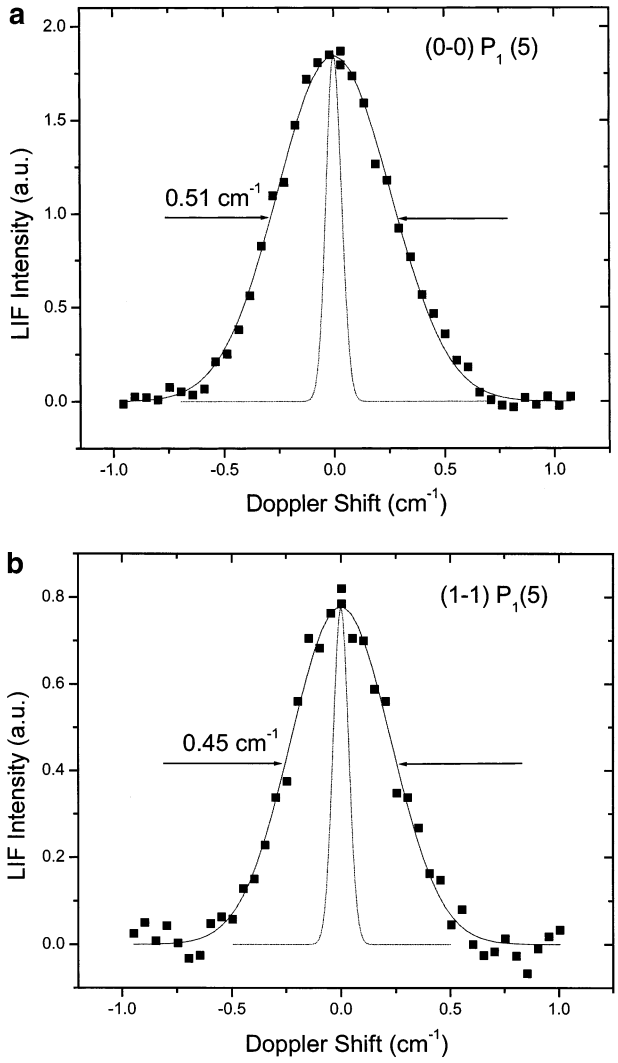

Figure 4. (a) Doppler profile of the $P_1(5)$ rotational line of the (0,0) transition of OH in the spectrum. The solid line drawn through the data points represents a Gaussian fit to the data points. The dotted line represents the instrument function (fwhm = 0.07 cm^{-1}). (b) Doppler profile of the $P_1(5)$ rotational line of the (1,1) transition of OH in the spectrum. The solid line drawn through the data points represents a Gaussian fit to the data points. The dotted line represents the instrument function (fwhm = 0.07 cm^{-1}).

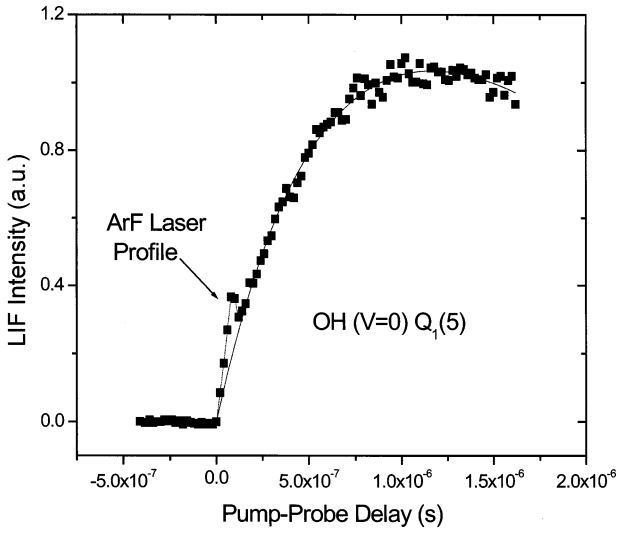

Figure 5. LIF intensity of OH generated in the dissociation of acetaldoxime as a function of the pump−probe delay. The acetaldoxime pressure is 10 mTorr, and the ArF laser fluence is 0.1 mJ cm^{-2}.

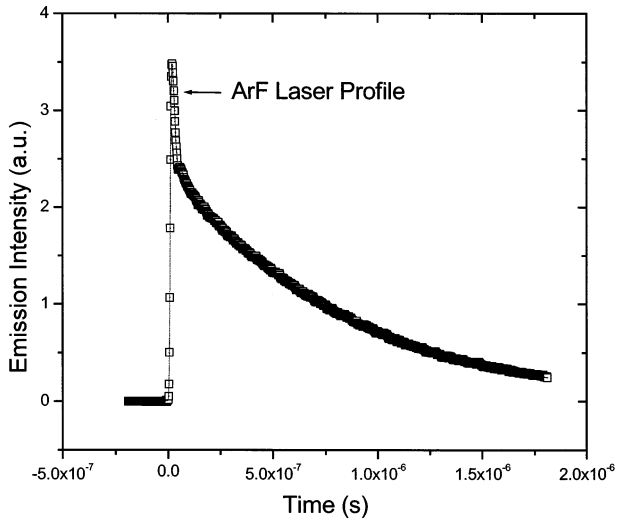

Figure 6. Emission intensity at 310 nm from the 193 nm ArF laser-excited acetaldoxime as a function of time. The acetaldoxime pressure is 10 mTorr, and the ArF laser fluence is 0.1 mJ cm^{-2}.

laser fired 500 ns before the photolysis laser, and subsequent data points were taken at 20 ns intervals afterward, which are averaged over 100 pulses. The measurements were carried out at a acetaldoxime pressure of 10 mTorr and at an ArF laser fluence of 0.1 mJ cm^{-2}. Several other intense rotational lines, mainly the strong lines of the Q_1 and P_1 branch of the (0,0) transition, were also measured as a function of the delay. It was found that the time-dependent signal intensities were independent of the rotational lines probed (4 or 6). This suggests that no significant rotational relaxation occurs on the above time scale.

The fast buildup of the OH signal is due to OH fragments generated in the dissociation of acetaldoxime, and a slow decay is observed afterward due to the diffusion of the nascent OH fragments. The average dissociation rate constant, *k*, of acetaldoxime was computed by fitting the time-dependent data (Figure 5) to a function

$$I(t) = A[1 - \exp(-kt)] - Dt \qquad (3)$$

where *A* is a fitting parameter and *D* is related to the diffusion coefficient. The dissociation rate constant of acetaldoxime is obtained as $(1.53 \pm 0.3) \times 10^6$ s^{-1}.

In another study, the 193 nm ArF excimer laser radiation was varied from 10 to 100 μJ/pulse and the OH LIF intensity of the $Q_1(5)$ rotational line was monitored as a function of the excimer laser fluence. The log−log plot of LIF signal vs photolysis energy yields a slope of 1.1 ± 0.1. This indicates that the OH radicals are produced in a single photon process.

3.4. Luminescent Emission from the Excited Acetaldoxime. On 193 nm laser excitation of acetaldoxime, a weak emission is observed in the 310 nm wavelength region. The emission spectrum could not be observed because of poor signal-to-noise ratio; however, the temporal profile of the emission was taken at 310 nm for obtaining the lifetime of the emitting species. A typical decay profile with a single exponential fit is shown in Figure 6. The decay constant of the emission was found to be $(1.2 \pm 0.3) \times 10^6$ s^{-1}. The observed emission may be from either an excited state parent molecule or an excited

product. The log−log plot of the emission signal against laser intensity showed a slope of 0.9 ± 0.1, which suggests that it is a single photon process. Because of energetic constraints, the observed emission at 310 nm precludes an excited product fragment.

For acetaldoxime, the assignment of the far ultraviolet spectra is reported,[20] where the singlet excited states (S_2) arise from a $\pi \rightarrow \pi^*$ transition of the C=N group at 180 nm, and the proximity $n \rightarrow \pi^*$ transition (S_1) comes as a shoulder at 210 nm. Although we have no knowledge about the triplet energy level of acetaldoxime, it is expected to be in the higher wavelength region, and the observed emission at 310 nm is tentatively assigned to the triplet excited state (T_1) of the acetaldoxime molecule. The photoexcitation scheme of acetaldoxime to the S_2 state, followed by internal conversion to the S_1 singlet excited state and further followed by an ISC to the T_1 triplet excited state, is shown above in Figure 1. On irradiation of acetaldoxime at 193 nm, we find similarity between the OH formation rate constant, $k = (1.5 \pm 0.3) \times 10^6$ s^{-1}, and the emission decay rate constant, $k = (1.2 \pm 0.3) \times 10^6$ s^{-1}, within experimental uncertainty limits. There is a competition between the emission and the dissociation from the triplet excited state, and the rate is determined by one of these. Assuming that the triplet state of acetaldoxime has approximately an energy level at 92 kcal mol^{-1}, which is equivalent to the photon energy of 310 nm emitted by an excited acetaldoxime, the OH formation rate constant, $k = (1.5 \pm 0.3) \times 10^6$ s^{-1}, fits well with the RRKM computation (cf. Section 3.5) of the triplet state dissociation, with a threshold dissociation energy as 49 kcal mol^{-1}. This value is quite reasonable as compared to that of the ground state threshold dissociation energy of 67 kcal mol^{-1}. Further work is needed to unambiguously assign the observed emission.

3.5. Evaluation of the Rate Constant Using RRKM Theory. The rate of formation of the nascent dissociation product OH, from the highly energized acetaldoxime produced by fast internal conversion of acetaldoxime molecules excited by a 193 nm photon, can be obtained by RRKM calculations. If the internal energy (E^*) of a molecule exceeds the dissociation energy E_o, the molecule is capable of spontaneous decomposition to fragments. The unimolecular decomposition rate $k(E^*)$ in a RRKM approximation[16] is described by the expression

$$k(E^*) = \frac{gQ^{\dagger}G(E^{\dagger} = E^* - E_o)}{QhN(E^*)} \qquad (4)$$

where $N(E^*)$ is the density of states for the molecule at E^*. $G(E^{\dagger})$ is the sum of state of critical configuration up to an excess energy $E^{\dagger}$, g is the reaction path degeneracy, and $Q^{\dagger}/Q$ is the ratio of adiabatic partition functions. Sums and densities of states are calculated by using the Whitten−Rabinovitch method.[16] The threshold energy for the dissociation of acetaldoxime is taken as 66.6 kcal mol^{-1}. A frequency factor of $\log A(s^{-1}) = 13.8$ is used, by following the reported unimolecular dissociation data of acetaldoxime[17] and an improved estimation over it by Benson and O'Neal.[12] The acetaldoxime vibrational frequencies are obtained from HF/6-311G** level calculation[18] (Gaussian 92) of structural optimization and normal modes, which are corrected with a factor of 0.89. The N−O stretching mode at 990 cm^{-1} becomes the reaction coordinate, and some of the vibrational frequencies are adjusted until agreement is reached between the A factor and the predicted entropy of activation.

The total energy of the acetaldoxime molecule after absorbing a photon is $E_{tot} = h\nu + E_{th}$. E_{th} is the thermal energy of the molecule at room temperature, obtained as

$$\langle E_{th} \rangle = KT\sum(h\nu_i/kT)/[\exp(h\nu_i/kT) - 1] \qquad (5)$$

where ν_i is the vibrational frequency of the molecule. Following rapid internal conversion after absorbing a 193.3 nm photon, the E_{tot} of acetaldoxime is 148.8 kcal mol^{-1}, which corresponds to a RRKM unimolecular dissociation rate constant of 1.2×10^{10} s^{-1}. This dissociation rate is found to be 4 orders of magnitude higher than the experimentally measured value, observed by our time-resolved pump−probe delay experiment.

TABLE 1: Parameters Used in RRKM Calculations

vibrational wavenumbers (cm^{-1})	
triplet state acetaldoxime molecule	activated complex
3700, 3000, 2890(3), 1650, 1400(3), 1300, 1150(2), 980, 950(3)*, 800(3)*, 500 and 140	as for molecule except those with asterisk replaced by 900(3), 635(3) and 980 dropped to become reaction coordinate
	$\log(A/s^{-1}) = 13.83$
	excess energy = 56.6 kcal mol^{-1}
	reaction path degeneracy = 1
	ratio of adiabatic partition functions, $Q^{\dagger}/Q = 1.2$

We repeated the above RRKM calculation for the triplet state of acetaldoxime, with the threshold dissociation energy as a variable parameter. Using 56.6 kcal mol^{-1} of excess energy available to the triplet acetaldoxime, the observed dissociation rate constant of the acetaldoxime, 1.53×10^6 s^{-1}, corresponds to the triplet state threshold dissociation energy at 49.2 kcal mol^{-1}. This seems quite reasonable while compared with the ground state threshold dissociation energy of 66.6 kcal mol^{-1}. Here, the triplet state of acetaldoxime is assumed to have approximately an energy minimum of 92.2 kcal mol^{-1}, which is equivalent to the photon energy of 310 nm emitted by the excited acetaldoxime. Thereby, the excess energy available to the triplet acetaldoxime is 56.6 kcal mol^{-1}. A frequency factor of $\log A(s^{-1}) = 13.8$ is used. The vibrational frequencies of the triplet state of acetaldoxime are obtained from a HF/6-311G** level calculation[18] (Gaussian 92) and corrected with a factor of 0.89. Here, the N−O stretching mode at 980 cm^{-1} becomes the reaction coordinate and vibrational frequencies of six modes are adjusted until agreement is reached between the A factor and the predicted entropy of activation. The frequencies taken for the triplet state acetaldoxime, its activated complex, and other parameters used in the RRKM calculations are given in Table 1.

3.6. Dissociation Energy Dynamics. The observation of 1.5% of the OH produced in the $\upsilon = 1$ corresponds to a vibrational temperature of $T_V = 1240 \pm 120$ K. This translates to an average vibrational energy in OH to be $E_V = 0.2$ kcal mol^{-1}. The measured distribution of rotational states, characterized by a rotational temperature T_{rot} of 1200 ± 120 K at $\upsilon = 0$ and T_{rot} of 990 ± 100 K at $\upsilon = 1$, respectively, corresponds to an average rotational energy of OH, $E_R = 2.4$ kcal mol^{-1}. The observation of OH translation by Doppler spectroscopy is found to fit with a Maxwell−Boltzmann velocity distribution, which corresponds to a release of an average translational energy of about 39.6 kcal mol^{-1} in the center of mass coordinate of the product fragments. While the above-mentioned energy associated with the rovibrational degrees of freedom of OH and overall translational energy for both of the photofragments, subtracted from the total available product energy 82.2 kcal mol^{-1}, it gives

us an internal energy of the $CH_3-CH{=}N$ radical to be about 40 kcal mol^{-1}. This is in contrast to the statistical energy distribution,[19] which suggests that about 62.6 kcal mol^{-1} remains as internal energy of the product radicals and 19.6 kcal mol^{-1} with the kinetic energy of the photofragments, out of the 82.2 kcal mol^{-1} of excess energy available from the primary photodissociation reaction I. Imparting such a large amount of translation energy into the N−O bond fission products suggests that the dissociation of acetaldoxime occurs on the excited state potential energy surface. Similar observation of large translational energy imparted with the C−C bond fission products (50 kcal mol^{-1} as translation energy out of 54 kcal mol^{-1} available energy) generated from the excited state dissociation have been reported by Butler and co-workers.[21] We have recently reported[22] the imparting of 36 kcal mol^{-1} translation energy out of 38 kcal mol^{-1} available energy in the C−O bond fission products from an excited state of 3-butenoic acid.

4. Conclusions

The photodissociation of acetaldoxime ($CH_3-CH{=}N-OH$) has been demonstrated by excitation with an ArF excimer laser, generating $CH_3-CH{=}N$ and OH radicals as primary products. The rovibrational spectroscopy of OH radical is studied by LIF. Most of the OH is formed in the ground vibrational state, and only 1.5% is formed in the $v = 1$ state, giving a vibrational temperature (T_{vib}) of 1240 ± 120 K. The rotational state distribution of OH is found to fit a Boltzmann distribution, characterized by a rotational temperature (T_{rot}) of 1200 ± 120 K for $v = 0$ and T_{rot} of 990 ± 100 K for $v = 1$ vibrational states, respectively. No preferential OH formation in either spin doublets or Λ doublets could be observed. By analysis of the OH rotational Doppler line-widths, the relative translational energy associated with the photofragments in the center-of-mass coordinate is found to be 40.0 ± 5.0 and 32.2 ± 4.0 kcal mol^{-1}, respectively, for the $v = 0$ and $v = 1$ states of OH. The real time formation of OH showed a dissociation rate constant of the acetaldoxime to be $(1.5 \pm 0.3) \times 10^6$ s^{-1}. The above dissociation rate vis-à-vis statistical RRKM theory suggests that acetaldoxime dissociates from the triplet state with a threshold dissociation energy of 49 kcal mol^{-1}. The decay of the acetaldoxime emission at 310 nm with a rate constant, $k = (1.2 \pm 0.3) \times 10^6$ s^{-1}, similar to that of its dissociation to form OH, suggests that both of the competitive decay processes occur from the same triplet excited state. The results clearly indicate that on photoexcitation at 193 nm, the $^1(\pi, \pi^*)$ excited acetaldoxime undergoes ISC to generate a highly energized triplet molecule, which is followed by photon emission or dissociation.

Acknowledgment. I thank Dr. T. Mukherjee and Dr. A. V. Sapre for their keen interest in this work. It is a pleasure to acknowledge the valuable discussions with Dr. J. P. Mittal and his kind support.

References and Notes

(1) Owrutsky, J. C.; Baronavski, A. P. *J. Chem. Phys*. **1999**, *110*, 11206.
(2) Kim, S. K.; Petersen, S.; Zewail, A. H. *J. Chem. Phys*. **1995**, *103*, 477.
(3) North, S. W.; Blank, D. A.; Gezelter, J. D.; Longfellow, C. A.; Lee, Y. T. *J. Chem. Phys*. **1995**, *102*, 4447.
(4) Nadler, I.; Mahgerefteh, T.; Reisler, H.; Wittig, C. *J. Chem. Phys*. **1985**, *82*, 3885.
(5) Zare, R. N. *Faraday Discuss. Chem. Soc*. **1986**, *82*, 391.
(6) Chowdhury, P. K.; Upadhyaya, H. P.; Naik, P. D. *Chem. Phys. Lett.* **2001**, *344*, 298.
(7) Chowdhury, P. K. *J. Phys. Chem. A* **2002**, *106*, 6223.
(8) Chowdhury, P. K.; Upadhyaya, H. P.; Naik, P. D.; Mittal, J. P. *Chem. Phys. Lett.* **2002**, *351*, 201.
(9) Chowdhury, P. K.; Upadhyaya, H. P.; Naik, P. D.; Mittal, J. P. *Chem. Phys. Lett.* **2002**, *356*, 476.
(10) Diau, E. W. G.; Kotting, C.; Zewail, A. H. *ChemPhysChem* **2001**, *2*, 273.
(11) Diau, E. W. G.; Kotting, C.; Zewail, A. H. *ChemPhysChem* **2001**, *2*, 294.
(12) Benson, S. W.; O'Neal, H. E. *Natl. Stand. Ref. Data Ser. (US, Natl. Bur. Stand.)* **1970**, 21.
(13) Dagdigian, P. J.; Anderson, W. R.; Sausa, R. C.; Miziolek, A. W. *J. Phys. Chem.* **1989**, *93*, 6059.
(14) Dieke, G. H.; Crosswhite, H. M. *J. Quant. Spectrosc. Radiat. Transfer* **1962**, *2*, 97.
(15) Chidsey, J. L.; Crosley, D. R. *J. Quant. Spectrosc. Radiat. Transfer* **1980**, *23*, 187.
(16) Robinson, P. J.; Holbrook, K. A. *Unimolecular Reactions*; Wiley-Interscience: New York, 1972.
(17) Pratt, G. L.; Purnell, J. H. *Trans. Faraday Soc*. **1962**, *58*, 692.
(18) Frisch, M. J.; et al. *Gaussian 92*, revision E1; Gaussian: Pittsburgh, PA, 1992.
(19) Campbell, R. J.; Schlag, E. W. *J. Am. Chem. Soc*. **1967**, *89*, 5103.
(20) Dargelos, A.; Sandorfy, C. *J. Chem. Phys*. **1977**, *67*, 3011.
(21) Kitchen, D. C.; Forde, N. R.; Butler, L. J. *J. Phys. Chem. A* **1997**, *101*, 6603.
(22) Chowdhury, P. K. *J. Chem. Phys.* Submitted for publication.